Journal of Alloys and Compounds 592 (2014) 306–312

Contents lists available at ScienceDirect

Journal of Alloys and Compounds

journal homepage: www.elsevier.com/locate/jalcom

Structural, dielectric and magnetic properties of $Bi_{1-x}Y_xFeO_3$ ($0 \leqslant x \leqslant 0.2$) obtained by acid–base co-precipitation

Leila María Saleh Medina [a], Guillermo A. Jorge [b], R. Martín Negri [a,*]

[a] Instituto de Química Física de Materiales, Ambiente y Energía (INQUIMAE), Departamento de Química Inorgánica, Analítica y Química Física, Facultad de Ciencias Exactas y Naturales, Universidad de Buenos Aires, Argentina
[b] Instituto de Ciencias, Universidad Nacional de General Sarmiento, Buenos Aires, Argentina

ARTICLE INFO

Article history:
Received 15 October 2013
Received in revised form 23 December 2013
Accepted 28 December 2013
Available online 9 January 2014

Keywords:
Multiferroic compounds
Bismuth–iron oxides
Yttrium substitution
Magnetization
Impedance analysis

ABSTRACT

Bismuth–iron oxides with partial substitution of bismuth by yttrium, referred as $(Bi_{1-x}Y_x)FeO_3$, were synthesized by simple-low cost acid–base co-precipitation method, which constitutes a difference with the currently used synthetic methods for obtaining $BiFeO_3$-doped compounds (e.g. polymer assisted sol–gel, solid state, microwave, etc.) Samples were characterized by XRD, EDS, SEM, TEM, DSC and FTIR.

The influence of yttrium (Y) substitution on magnetization curves of $(Bi_{1-x}Y_x)FeO_3$ powders were studied at room temperature by VSM. The particle size systematically decreases with the Y percentage. Ferromagnetic curves were obtained at room temperature for Y-percentage lower than 20% with relatively large values of the coercive field, H_c, which increases with Y-substitution, while for 20% yttrium a superparamagnetic behavior is observed.

The electrical impedance of compressed disks were investigated also by impedance analysis in the range 1Hz–1MHz and the results were successfully fitted by a simple parallel R–C model. The dc-leakage currents are lower than previously reported for $(Bi_{1-x}Y_x)FeO_3$ compounds and for most of the doped-$BiFeO_3$ ceramics. As a difference with the influence on the magnetic behavior, the doping with yttrium does not seem to have a large influence on the dielectrical properties. These results suggest that magnetization can be systematically modified by the relatively simple co-precipitation synthesis while keeping invariable the dielectrical properties.

1. Introduction

Multiferroic compounds are receiving increasing attention due to the possibility of modulating electrical properties using magnetic fields and vice versa. These properties are of high technological interest for potential applications in magnetoelectric sensors, magnetic memories and electromagnetic energy conversion. The challenge from the point of view of material science is to find compounds with the required properties: magneto-electrical coupling at room temperature, well-defined and stable structures at micro or nanolevels, and the appropriated values of some relevant magnitudes according to the target application (e.g. remanent magnetization, coercive field or dc-leakage currents). Although bismuth ferrites ($BiFeO_3$) present multiferroic properties at room temperature and are perhaps the most studied multiferroic materials, their applications are limited due to their very weak magnetic properties at those temperatures. In order to enhance the magnetic properties, the metal doping with partial substitution of bismuth (Bi) or iron (Fe) by different metals has received considerable attention [1–11]. The partial substitution of Bi by yttrium III (Y) appears as an interesting alternative [2,12], although establishing simple synthesis protocols is not an easy task. For instance, Bellaki et al. [12] observed that room temperature magnetization values increase when doping with low amounts of yttrium in $Bi_{0.98}Y_{0.02}FeO_3$ obtained by solution combustion method. Mishra et al. [2] obtained $(Bi_{1-x}Y_x)FeO_3$ compounds prepared by a metal ion ligand complex-based precursor-solution evaporation method, obtaining large broadening of the X-ray diffraction line profile when increasing the yttrium percentage from 0 to 0.15 assigned mainly to lattice strain effects. Gautam et al. [13] synthesized $BiFeO_3$ oxides substituted with Y(II) instead of Y(III) by a sol–gel route, obtaining simultaneously other oxides (impurities), and very different lattice parameters for the $BiFeO_3$-Y(II) phase in comparison with those obtained by Mishra et al. for $BiFeO_3$-Y(III). On these bases, we decided to synthesize $(Bi_{1-x}Y_x)FeO_3$ compounds by a simpler route, using the acid–base co-precipitation method, which is well-known for obtaining nanoparticles and has been used in our group for synthesizing superparamagnetic and ferromagnetic compounds [14–19]. In the co-precipitation method bismuth is systematically substituted by yttrium (III), Y(III), and the percentage of

* Corresponding author. Address: Ciudad Universitaria, Pabellón II, INQUIMAE, C1428EGA, Buenos Aires, Argentina. Tel.: +54 11 4576 3358; fax: +54 11 4576 3341.
E-mail address: rmn@qi.fcen.uba.ar (R. Martín Negri).

0925-8388/$ - see front matter © 2014 Elsevier B.V. All rights reserved.
http://dx.doi.org/10.1016/j.jallcom.2013.12.243

Y(III)-substitution is referred as X(=100x). Hence, the aim of this work is to analyze the effect of yttrium substitution (X) on the structure, magnetic and dielectric properties, and *dc*-conductivity at room temperature of the $(Bi_{1-x}Y_x)FeO_3$ compounds obtained by the selected synthetic procedure.

2. Experimental section

2.1. Synthesis of $(Bi_{1-x}Y_x)FeO_3$

The chemical co-precipitation method was used for the synthesis of $(Bi_{1-x}Y_x)$-FeO_3 nanoparticles [20]. Stoichiometric amounts of $Bi(NO_3)_3{\cdot}5H_2O$, $FeCl_3{\cdot}6H_2O$/$Fe(NO_3)_3{\cdot}9H_2O$ and Y_2O_3 were successively dissolved in 25 mL of HNO_3 65% under stirring at 60 °C until complete dissolution of all the compounds. After reaching room temperature (25 ± 2) °C, this mixture solution was placed on a separating funnel and then added drop-by-drop to 200 mL of NH_3 (3 M) at room temperature and at high speed stirring. The pH of this suspension was kept constant during the whole process of addition (pH = 9.3) by adding drops of ammonia. The apparition of reddish particles occurred immediately. This suspension was kept vigorously stirred at room temperature for 2 h. Then particles were separated from the reaction medium by centrifugation at approximately 12,000 G for 20 min. The obtained precipitates were washed with MilliQ water. Washing and centrifugation cycles (always at 12,000 G) were repeated until reaching pH = 7 in the supernatant. Afterwards, the particles were dried in a vacuum oven at 50 °C for 24 h. Finally, a fraction of the dried material was calcined at 500 °C. This temperature was determined as the appropriated to obtain the expected phase by recording XRD diffractograms of materials calcined at different temperatures.

In order to obtain disks of multiferroic material for electrical measurements, about 500 mg of $(Bi_{1-x}Y_x)FeO_3$ powders were compressed in a pellet making die at 100 kgf. Several disks of different areas (A) and thickness (L) were obtained by this procedure (A: 1.33–2.00 cm^2; L: 400–500 μm).

2.2. Instrumentation

X-ray powder diffraction analysis (XRD) was performed with a Philips X-Pert diffractometer using Cu Kα radiation (λ = 0.154056 nm). The average crystallite sizes were determined by the Debye–Scherrer equation using the (0 1 2) peak, fitted with a Lorentzian curve to obtain the full width at the half maximum height (FWHM). The morphology of the powders was studied by Scanning Electron Microscopy (SEM) using a Field Emission Scanning Electron Microscope (FESEM; Zeiss Supra 40 Gemini). The size distribution was determined in each case by counting on at least 300 particles. Energy-Dispersive X-ray Spectroscopy (EDS) experiments were performed with an Oxford Instrument detector, model INCAx-Sight.

Fourier Transformed Infra-Red (FTIR) spectra were recorded with a Nicolet 8700 equipment incorporating the samples into KBr pellets and using transmission technique. Differential Scanning Calorimetry (DSC) was performed with a Shimadzu DSC-50 equipment. The powders were heated to 500 °C at a rate of 10 °C/min and with a rate flow of 30 mL/min of N_2(g).

A LakeShore 7400 Vibrating Sample Magnetometer (VSM) was used for recording magnetization curves at room temperature. Powder samples were weighted (10–80 mg) and then packed with Teflon tape and mounted on the VSM sample-holder. The magnetization curves were recorded from positive saturation at 1.8 Tesla (T), in steps of 25 mT or less, with an integration constant of 10 s for each applied magnetic field.

A specially designed set up was used for measuring the electrical response of the disks at different applied pressures. The disks were placed between two metallic surfaces having similar areas to the disks (top and bottom electrodes) and a thin sheet of high purity gold was placed between the disk and the electrodes. Then a small pressure was applied between the electrodes to ensure good contacts and the force on the disks was measured with a force sensor. This set up was used for measuring electrical impedance and leakage currents. Electrical impedance measurements between 0.1 Hz and 1 MHz were performed with a TEQ 4 (Argentina) potentiostat. The leakage current was measured as function of the applied dc voltage with a Keithley 193A System DMM nanoamperemeter.

3. Results and discussions

3.1. Chemical and morphological characterization of $(Bi_{1-x}Y_x)FeO_3$ powders

The room temperature FTIR spectra are shown in Fig. 1. The absorption peaks in the range 400–600 cm^{-1} correspond to the Fe–O bending (~430 cm^{-1}), Fe–O stretching (~525 cm^{-1}) and Bi/Y–O (~490 and ~590 cm^{-1}) vibrations, being characteristic of octahedral arrangements in the perovskite structure [2,21]. The

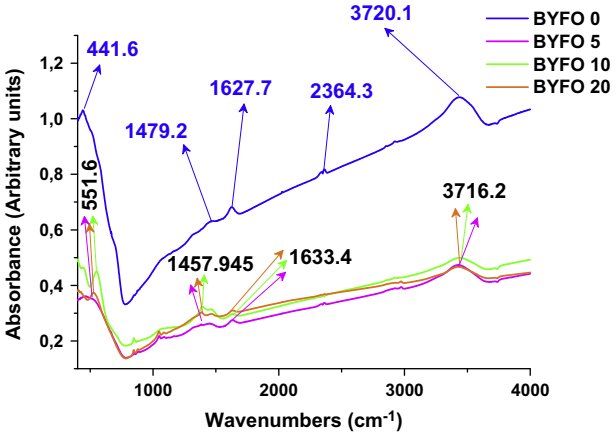

Fig. 1. IR absorption spectra of $Bi_{1-x}Y_xFeO_3$ powders calcined at 500 °C.

peaks at around 1400 cm^{-1} can be due to trapped nitrates while the ones between 800–1000 cm^{-1} may correspond to adsorbed molecular oxygen [1].

Heat absorption peaks were detected by DSC in all samples at temperatures identified as the Néel temperature, T_N, assigned to the antiferromagnetic transition (T_N between 309–370 °C and heat transition between 3.8 and 6.3 J/g, depending on the sample (Fig. 2). The value of T_N for X = 0 is in agreement with previously reported values for samples obtained using other methods of synthesis [22–24].

The X-ray powder diffraction patterns (XRD, Fig. 3) indicate that the $(Bi_{1-x}Y_x)FeO_3$ nanoparticles, for all values of x (x = 0, 0.05, 0.10, 0.20), are essentially crystalline single phase with XRD peaks corresponding to perovskite structure (JCPD 01-072-7678).

Apparition of segregated phases such as Y_2O_3 or Bi_2O_3 is not observed and signals corresponding to $Bi_2Fe_4O_9$, $Bi_{25}FeO_{40}$ or $Bi_{24}Fe_2O_{39}$ (reported by Mishra et al. [2] and Hardy et al. [25]) has not been detected.

The position and relative intensities of the peaks for $BiFeO_3$ (referred to BYFO-0 in Fig. 3) are coincident with those reported by Shami et al. [1]. The XRD patterns shown in Fig. 3 change with the percentage of yttrium substitution X. The angles at which the peaks appear are slightly modified with the percentage of yttrium (except for X = 20 where bigger shifts are observed) but the relative intensities of the peaks change with X. For instance, the intensity ratio between the peaks at 2θ = 22.5° and 32°, ($I_{22.5}/I_{32}$) decreases with X. This decrease in peak intensities with increasing amount

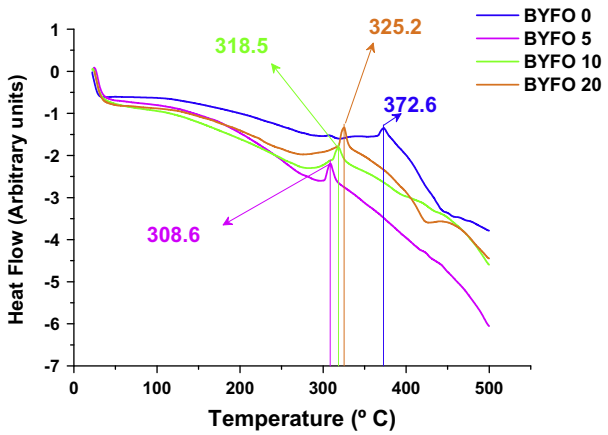

Fig. 2. DSC curves of $Bi_{1-x}Y_xFeO_3$ powders calcined at 500 °C.

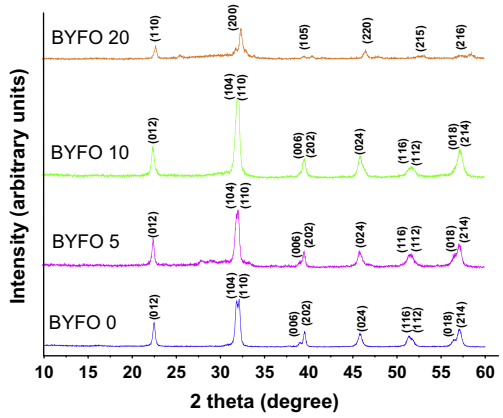

Fig. 3. XRD patterns of $(Bi_{1-x}Y_x)FeO_3$, referred as BYFO-X. Peaks of rhombohedral $BiFeO_3$ are labelled with JCPD card No. 01-072-7678 [1]. Peaks corresponding to tetragonal phase are labelled according to Mishra et al. [2].

of yttrium can be due to higher scattering on some particular planes when introducing Y(III) in Bi(III) sites. Also, it is possible that Bi(III) ions move to interstitial sites which may render into distortion of the diffractogram, as reported in doped SnO_2 [26].

The most noticeable alteration is for $X = 20$, where the change in the number of peaks is clearly noticeable. Similar changes were already reported by Mishra et al., assigning these changes to distortion of the rhombohedral structure induced by the presence of Y in samples with $X > 10$. The distortion of the XRD pattern when increasing Y substitution is in agreement with a continuous structural phase transition, as reported in many works when doping with rare earths [5].

The crystallite sizes, obtained by Debye–Scherrer for $X \leqslant 10$, and the particle size distribution are shown in Table 1 as function of X. Several SEM images (Fig. 4) were analyzed to obtain the particle size distribution histograms (Fig. 5).

The mean particle size, $\langle d \rangle$ and standard deviation, were calculated by fitting the histograms with a Lorentzian distribution (Table 1 and Fig. 5). The crystallite size is smaller than the media particle size ($\langle d \rangle$) for $X = 0$–10. The values of a,b,c for $X \leqslant 10$ are similar to those previously reported for BYFO compounds synthesized by different methods [2,12,22,27].

The main conclusion of this section is that samples obtained by co-precipitation do not present other Bi or Y oxide phases already reported in other cases. Crystallinity and purity remains highly satisfactory, although doping with Y induces small structural transformations (except at $X > 10$ where structural changes are relevant) and systematic decrease of the particle size with X (including $X = 20$).

3.2. Magnetic properties of $(Bi_{1-x}Y_x)FeO_3$ powders

Fig. 6 shows the magnetization curves at 25 °C varying with X.

Table 1
Structural and morphological parameters of BYFO compounds.

X[a]	Crystallite size[b] (nm)	$\langle d \rangle$[c] (nm)	σ[d] (nm)	a[e] (Å)	b[e] (Å)	c[e] (Å)
0	27.5 ± 0.3	38.4 ± 0.4	7.1 ± 0.5	4.8	4.8	13.8
5	24.3 ± 0.5	27.9 ± 0.4	5.2 ± 0.5	4.6	4.6	14.9
10	21.5 ± 0.4	21.9 ± 0.3	5.6 ± 0.4	4.8	4.8	13.8
20	–	11.4 ± 0.3	2.7 ± 0.3	3.3	3.3	8.4

[a] Yttrium percentage.
[b] From Debye–Scherrer equation.
[c] Particle size distribution centre.
[d] Standard deviation, respectively.
[e] Unit cell parameters.

One central feature to be remarked is the observation of weak ferromagnetic behavior for $X = 0$ to $X = 10$ with relatively higher values of the coercive field, H_c (Table 2) than those previously reported for $BiFeO_3$ [5–9,28] and $(Bi_{1-x}Y_x)FeO_3$ compounds [2] of similar crystallite sizes obtained using other synthetic routes. The values of H_c reported in Table 2 are larger than those reported by [5] when doping with Eu at $X < 10\%$ (although these authors obtained very large values of H_c for $X > 10\%$, where X is the percentage of Eu substitution using a different synthesis). It is also important to remark that the intriguing switching behavior of the magnetization reported by Mishra et al. [2] in $Bi_{1-x}Y_x)FeO_3$ compounds (referred as metamagnetic transition) was not observed. The values of the remanent magnetization, M_r, are similar to previously reported [5,6,8,28–30]. Thus, the main observed characteristic is the large values of H_c obtained by the co-precipitation method, which increase from $X = 0$ to $X = 10$. That is, the synthesized compounds behave as hard ferromagnetic materials for $X \leqslant 10$. On the other hand, superparamagnetic behavior was obtained for $X = 20$. Finally, it can be noted the magnetization at 20 kOe increases with X. These characteristics are discussed in the following paragraph.

Although the full understanding of the multiferroic behavior of $BiFeO_3$-doped compounds is controversial, there is a general agreement that bulk $BiFeO_3$ has an antiferromagnetic order (AFM) at room temperature. The crystal structure of $BiFeO_3$ is consistent with a G-type AFM ordering along the $[0\,0\,1]_{hex}$ axis in the hexagonal representation, which in principle should render to a null spontaneous magnetization. However, magnetoelectric effects due to the presence of spontaneous electrical polarization [31], generates exchange interactions and spin–orbit interactions that partially destroy the perfect AFM ordering, inducing a small magnetic moment [28]. But, the direction of this moment rotates forming a so-called spin cycloid with a wave-vector along the $[1\,1\,0]_{hex}$ axis with a 64 nm wavelength [31]. Then, if the wave-vector is not disrupted by imperfections, grain borders, etc., within a length smaller than 64 nm, the spin cycloid completes a wavelength and this full helicoidal order results again in vanishing the magnetization. On the other hand, if the spin-cycloid modulation is disrupted at length shorter than 64 nm, the helicoidal order is suppressed and a weak ferromagnetism is then predicted. In fact, the change from AFM behavior to weak ferromagnetism (FM) was observed when going from bulk or particles larger than 200 nm to particles lower than 70 nm [8,28]. Summarizing, the FM order observed in materials formed by particles with crystallite or particle sizes smaller than 60–70 nm is currently assigned to suppression of the complete spin cycloid at the particle or crystallite surface [32]. Hence, the effective model has been described as the superposition of an AFM core and a FM surface when particles are smaller than 64 nm. The observation of weak FM for particles with $X \leqslant 10$ is consistent with that model since the obtained particles presents crystallite and size particles lower than 64 nm. That is, this model suggest that the system can be represented by an AFM core superimposed with a FM surface (the AFM-helicoidal order is suppressed at the surface). This model is qualitatively in agreement with the results of Fig. 6 and Table 2 for $X \leqslant 10$.

The remarkable characteristic for $X \leqslant 10$ is that the obtained FM compounds display large values of H_c, which increase with X, from $X = 0$ to $X = 10$, followed by a transition to superparamagnetic behavior for $X = 20$. The increase of H_c from $X = 0$ to $X = 10$ suggests that particles are formed by several magnetic domains in the regime $X \leqslant 10$, where the origin of the large H_c can be assigned to the activation energy barrier for wall domain motion. The barrier for wall-domains motion is lower than the activation barrier for monodomain rotation, then if the number of monodomain particles increases when reducing the particle size, the activation barrier also increases, thus H_c increases when particle size decreases, as observed Fig. 6 and Table 2.

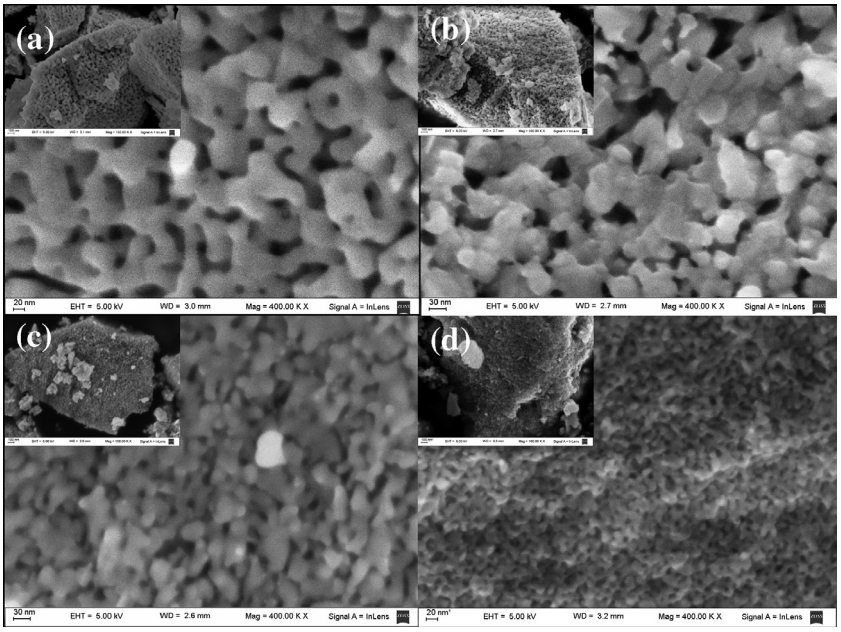

Fig. 4. SEM images of: (a) BYFO-0; (b) BYFO-5; (c) BYFO-10; (d) BYFO-20.

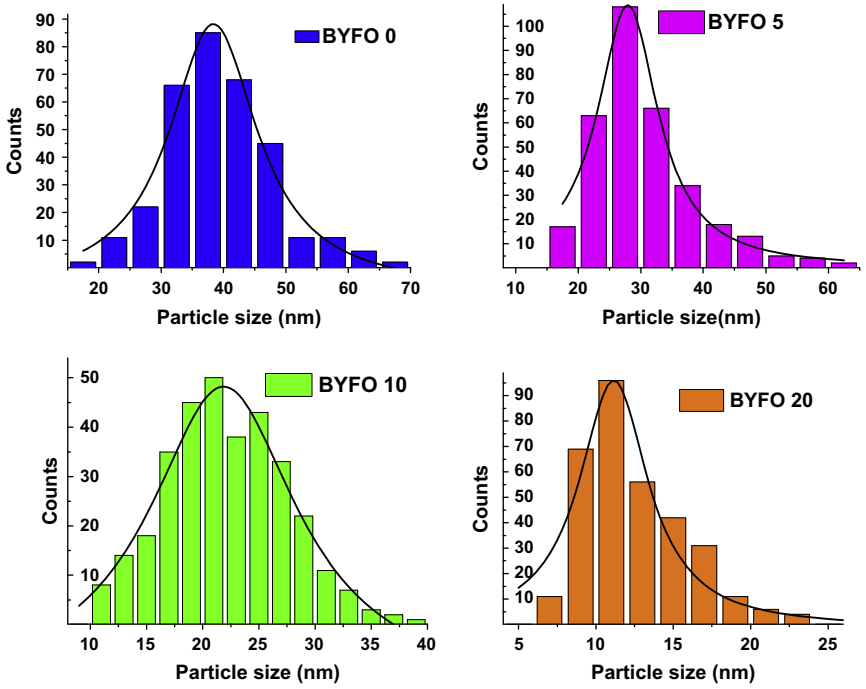

Fig. 5. Histograms of particle size distribution for the different $(Bi_{1-x}Y_x)FeO_3$ samples. The lines represent fits by a Lorentz distribution. In each case 300 particles were considered.

The other central characteristic is the observed superparamagnetic (SPM) behavior obtained for samples with $X = 20$. This samples have an average size diameter, $\langle d \rangle = 11$ nm which is much lower than the others obtained for $X \leqslant 10$ (Table 1). Changes of magnetic behavior for samples with $\langle d \rangle \leqslant 14$ nm have been reported by [28]. These authors propose that at those low size values the magnetism of $BiFeO_3$ samples can not be described by the model described in the previous paragraphs (AFM core superimposed with a FM surface) since distortions of the structure due to Y-doping expands to the whole particle at $\langle d \rangle \leqslant 14$ nm. In the present work, these low size values are reached for $X > 10$. Thus, the results presented are consistent with the proposal of Park et al. [28]. Interestingly, the magnetization observed at the largest magnetic field (e.g. $H > 10$ kOe) increases when $\langle d \rangle$ decreases (see Fig. 7a and b), in qualitative agreement with the whole model already described since reduction of the particle size has the effect of suppressing the AFM order, irrespectively of what order (FM or SPM) is created.

3.3. Electrical properties of compressed disks

Compressed disk of the powders calcined at 500 °C were prepared and their electrical properties were measured as described in Section 2.1. The obtained disks were sintered also at 500 °C.

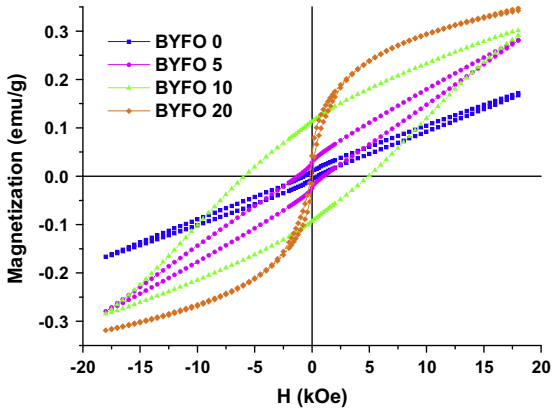

Fig. 6. Magnetization curves for the different $(Bi_{1-x}Y_x)FeO_3$ samples at 25 °C.

Table 2
Magnetic and electric parameter of BYFO compounds at 25 °C.

X[a]	H_c[b] (G)	M_r[c] (emu/g)	M (emu/g) at H = 20 kOe	ρ (MΩ cm)[d]	ε[e]
0	800	0.02	0.17	1.7 ± 0.1	16 ± 4
5	1000	0.03	0.28	2.20 ± 0.03	12 ± 3
10	5000	0.11	0.30	7.8 ± 0.1	13 ± 3
20	–	–	0.36	13.90 ± 0.01	14 ± 4

[a] Yttrium percentage.
[b] Coercive field.
[c] Remanent magnetization.
[d] Dc-electrical resistivity of compressed disks at 295 kPa extrapoled from impedance analysis.
[e] Dielectric constant of compressed disks measured at P = 295 kPa.

Calcination and/or sintering at higher temperatures (550–700 °C) generates apparition of new phases such as $Bi_2Fe_4O_9$ and $Bi_{25}FeO_{39}$ [20]. For that reason only samples sintered at 500 °C were used in the electrical studies (*dc* leakage currents and *ac* impedance analysis). The measured density of the compressed sintered disks is about 60–70% of the calculated density. It was not possible to obtain higher densities since sintering at higher temperatures was prevented by thermal degradation of the material as indicated above. As described in Section 2.1, a small pressure, P (in the range 20–300 kPa), was applied on the disks to improve the electrical contacts in all the electrical measurements.

3.3.1. DC leakage currents of compressed disks of $(Bi_{1-x}Y_x)FeO_3$

Fig. 8 shows the density current, J, as function of the applied *dc* electric field, E, usually referred as the leakage currents plots, for compressed disks of $(Bi_{1-x}Y_x)FeO_3$. No differences were observed in the electrical response (J–E response) between disks non-sintered and disks sintered at 500 °C.

Fig. 8a and b illustrate the low leakage currents of the samples, observed always in the several replicates prepared. In fact, the obtained leakage currents (or the slopes of J–E plots, dJ/dE, for $E \rightarrow 0$) are much lower than those previously reported for similar pellets of $BiFeO_3$ (X = 0) and many other rare-earth ions and alkaline-earth metal doped $BiFeO_3$ [5,9,33], except when comparing with the values obtained by Zhang et al [5] for $Bi_{1-x}Eu_xFeO_3$ for $x > 0.10$.

Fig. 8b shows that the J–E slope decreases with X; although that behavior was not always reproducible when considering several replicates, dJ/dE remained very low ($dJ/dE \approx 10^{-10}$ AV^{-1} cm^{-1}).

3.3.2. AC dielectric behavior of compressed $(Bi_{1-x}Y_x)$: FeO_3

The impedance data, $Z(\omega)$, were adjusted by a R//C model: $Z(\omega) = \frac{RZc}{R+Z_c}$ with $Z_c(\omega) = j\frac{1}{\omega C}$ ($\omega = 2\pi f$, being f the applied frequency) assuming constant values of the resistance, R, and

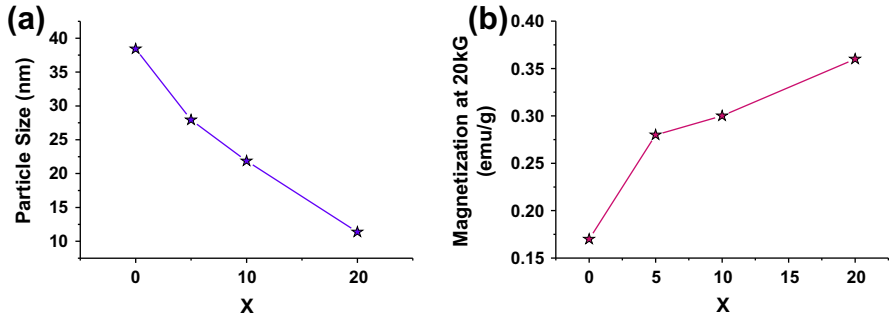

Fig. 7. (a) Average particle size, $\langle d \rangle$, vs. yttrium percentage, X. (b) Room temperature magnetization measured at 20 kOe vs. X.

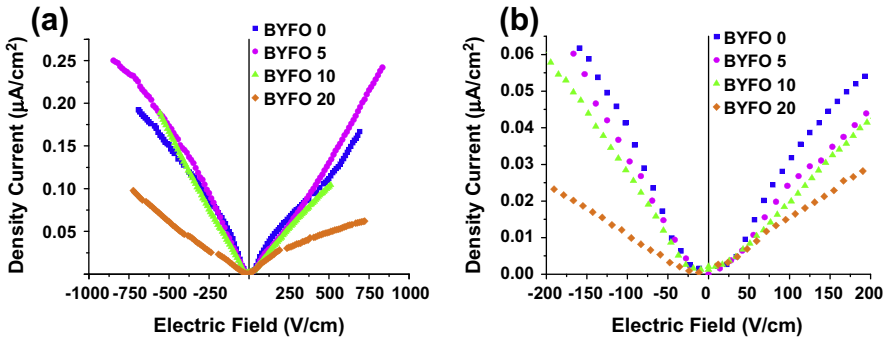

Fig. 8. (a) Density current, J, vs. *dc* electric field, E, for compressed disks of $(Bi_{1-x}Y_x)FeO_3$. (b) Amplification in the range 200 V/cm. A pressure of 37 kPa between contacts was applied.

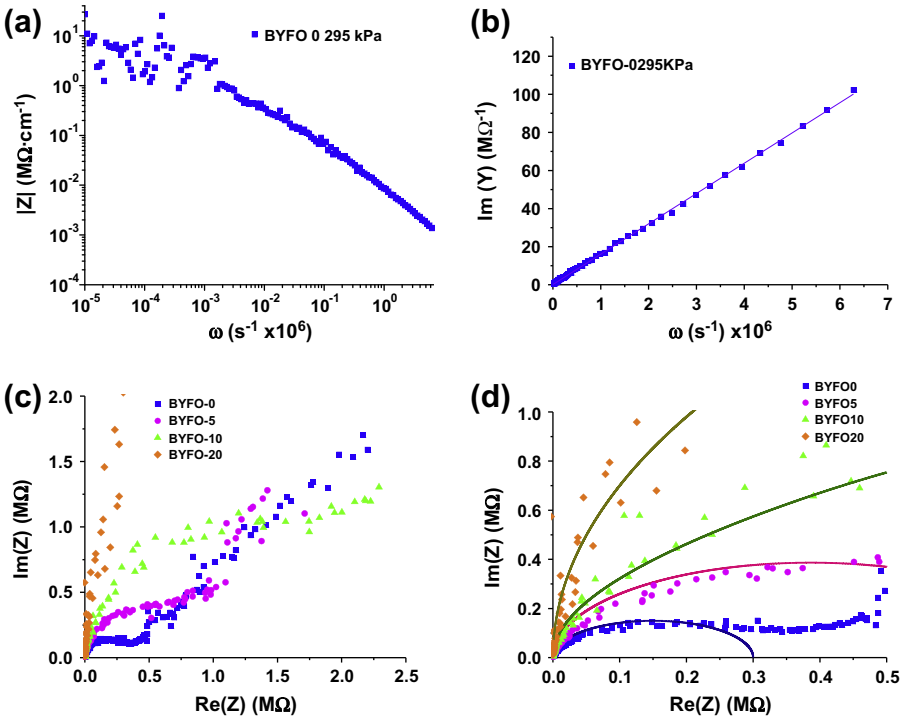

Fig. 9. (a) Impedance module vs. frequency of BYFO-0 compressed disks; (b) imaginary part of admittance vs. frequency of BYFO-0 compressed disks; (c) Nyquist plot of compressed disks of similar dimensions but different *X*; (d) amplification of Nyquist plot in the high-frequency range and simulated curves using a R//C model. In all cases the applied pressure was 295 kPa.

capacitance, *C*, at the low applied voltage used in the impedance experiments (5 V, which corresponds to E ≅ 100–125 V/cm, depending on the thickness of the sample). A small pressure was applied (and registered) on the compressed disks during measurements.

The absolute value of the imaginary part of the admittance ($Y \equiv \frac{1}{Z}$) follows a linear relationship with ω (Fig. 9b) whose slope is the capacitance, C, as predicted by the R//C model. The dielectric constant, ε, was calculated from $\varepsilon = \frac{C}{\varepsilon_0}(\frac{L}{A})$ where $\varepsilon_0 = 8.85\ 10^{-12}$ F/m is the vacuum permittivity, while *A* and *L* are the area and thickness of the sample disk, respectively. In the R//C model the dielectric constant ε is assumed to be independent of the frequency. The experimental results shown in Fig. 9a–d are in agreement with the proposed model.

From the impedance analysis is possible to recover not only the dielectric constant, ε, but also the electrical resistivity, ρ (see Table 2). As mentioned before, for a fixed pressure no variation of ε with *X* was observed. However it was observed that ρ increases systematically with *X*. It has been proposed [34] that the conduction mechanism of $BiFeO_3$ is related to the hopping of electrons from Fe^{2+} to Fe^{3+} when oxygen vacancies are present in the lattice, which act as bridges between Fe^{2+} and Fe^{3+}. Assuming this description as valid, a possible interpretation of the experimental observation that ρ increases with *X* is that the partial substitution of Bi by Y decrease the amount of defects in the solid, stabilizing the Fe(III) oxidation state, and disrupting the electron hopping.

4. Conclusions

$Bi_{1-x}Y_xFeO_3$ ($x = 0$–0.20, $X = 0$–20) were successfully synthesized by a simple co-precipitation method, obtaining pure single phase compounds. The obtained XRD patterns, EDS results, T_N values, FTIR spectra and SEM images are consistent with single phase high purity $Bi_{1-x}Y_xFeO_3$ samples, without observation of other phases. Thus, using the acid–base co-precipitation method it is possible to eliminate Bi-rich impurity phases that usually appears when other methods of synthesis are used. Doping with Y introduces small distortion of the crystalline structure, except for $X = 20$ where distortion is larger, with a systematic decrease of the particle size. In all cases particles lower than 40 nm are obtained. The suppression of the AFM order and the apparition of FM order (for $X \leqslant 10$) and a SPM order (for $X = 20$) can be assigned to the small particle sizes obtained. The relatively large coercive fields H_c, (in comparison with most of previously reported values for samples obtained using other synthetic routes) increases with *X*. These observations are consistent with the presence of multi magnetic domains in samples with $X \leqslant 10$. This is a significant feature of the synthesized samples concerning with applications in magnetic memories. The other central characteristic is that leakage currents are significantly lower than previously reported for this type of compounds, a relevant characteristic for capacitor design, with resistivities that decrease with *X*. For instance, when comparing with $BiFeO_3$ compounds substituted with samarium obtained from solid state reaction [6] the samples presented here have more than the double value of H_c and less than a half of the leakage current for the same substitution percentage. The impedance analysis is well described by a simple R//C model (with no significant changes of the dielectric constant with *X*) without needing of introducing any semi-empirical parameter which usually presents a lack of physical meaning.

Acknowledgements

GJ and RMN are research members of the Argentinean Research Council (CONICET). LMSM is a doctoral fellow of CONICET. Financial support was received from the University of Buenos Aires (UBACyT 2012–2015, 2002 01101 00098) and Ministry of Science, Technology and Innovations (MINCYT-FONCYT, PICT 2011-0377). The authors thank to Center of Advanced Microscopy (CMA), School of Sciences, University of Buenos Aires, for obtaining the

presented SEM images and the Low Temperature Physics Laboratory, School of Sciences, University of Buenos Aires for allowing accessing VSM facilities.

References

[1] M.Y. Shami, S. Awan, M. Anis-Ur-Rehman, J. Alloys. Comp. 509 (2011) 10139–10144.
[2] R.K. Mishra, D.K. Pradhan, R.N.P. Choudhary, A. Banerjee, J. Phys.: Condens. Matter 20 (2008) 45218.
[3] S. Chauhan, M. Kumara, S. Chhoker, S.C. Katyal, H. Singh, M. Jewariya, K.L. Yadav, Solid State Commun. 152 (2012) 525–529.
[4] D.H. Wang, W.C. Goh, M. Ning, C.K. Ong, Appl. Phys. Lett. 88 (2006) 212907.
[5] Y.S. Xingquan Zhanga, Xianjie Wanga, Yang Wangc, Zhu Wanga, J. Alloys. Comp. 507 (2010) 157–161.
[6] K.S. Nalwa, A. Garg, A. Upadhyaya, Mater. Lett. 62 (2008) 878–881.
[7] F. Azough, R. Freer, M. Thrall, R. Cernik, F. Tuna, D. Collison, J. Eur. Ceram. Soc. 30 (2010) 727–736.
[8] L. Luo, K. Shen, Q. Xu, Q. Zhou, W. Wei, M.A. Gondal, J. Alloys. Comp. 558 (2013) 73–76.
[9] P. Suresh, S. Srinath, J. Alloys Comp. 554 (2013) 271–276.
[10] G. Dhir, G.S. Lotey, P. Uniyal, N.K. Verma, J. Mater. Sci. Mater. Electron. (2013) 1–7.
[11] P. Uniyal, K.L. Yadav, Mater. Lett. 62 (2008) 2858–2861.
[12] M.B. Bellaki, V. Manivannan, C. Madhu, A. Sundaresan, Mater. Chem. Phys. 116 (2009) 599–602.
[13] A. Gautam, P. Uniyal, K.L. Yadav, V.S. Rangra, J. Phys. Chem. Solids 73 (2012) 188–192.
[14] M.M.R. José Luis Mietta, Paula Soledad Antonel, Oscar Perez, a Butera, Guillermo Jorge, Ricardo Martin Negri, Langmuir 28 (2012) 6985–6996.
[15] G.J. José, L. Mietta, Oscar E. Perez, Thomas Maeder, R. Martín Negri, Sens. Actuators A 192 (2013) 34.
[16] P.S. Antonel, G. Jorge, O.E. Perez, A. Butera, A.G. Leyva, R.M. Negri, J. Appl. Phys. 110 (2011) 043920.
[17] M.M. Ruiz, J.L. Mietta, P.S. Antonel, O.E. Pérez, R.M. Negri, G. Jorge, J. Magn. Magn. Mater. 327 (2013) 11–19.
[18] A. Butera, N. Álvarez, G. Jorge, M.M. Ruiz, J.L. Mietta, R.M. Negri, Phys. Rev. B 86 (2012) 144424.
[19] P.S. Antonel, R.M. Negri, A.G. Leyva, G.A. Jorge, Phys. B: Condens. Matter 407 (2012) 3165–3167.
[20] W.W. Hua Ke, Yuanbin Wang, Jiahuan Xu, Dechang Jia, Zhe Lu, Yu Zhou, J. Alloys Comp (2011) 2192–2197.
[21] C.J. Chen C, S. Yu, L. Che, Meng Z, J. Cryst. Growth 291 (2006) 135.
[22] S.M. Selbach, M.-A. Einarsrud, T. Tybell, T. Grande, J. Am. Ceram. Soc. 90 (2007) 3430–3434.
[23] A.S.T. Karthik, V. Kamaraj, V. Chandrasekeran, Ceram. Int. 38 (2012) 1093–1098.
[24] I.S. Kambiz Kalantari, Derek C. Sinclair, Paul A. Bingham, Jan Pokorný, Ian M. Reaney, J. Appl. Phys. 111 (2012) 064107.
[25] A. Hardy, S. Gielis, H.V.D. Rul, J. D'haen, M.K.V. Bael, J. Mullens, J. Eur. Ceram. Soc. 29 (2009) 3007–3013.
[26] J. Joseph, V. Mathew, K.E. Abraham, Chin. J. Phys. 45 (2007) 84–97.
[27] Y. Wang, G. Xu, Z. Ren, X. Wei, W. Weng, P. Du, G. Shen, G. Han, Ceram. Int. 34 (2008) 1569–1571.
[28] T.J. Park, G.C. Papaefthymiou, A.J. Viescas, A.R. Moodenbaugh, S.S. Wong, Nano Lett. 7 (2007) 766–772.
[29] W. Cai, C. Fu, W. Hu, G. Chen, X. Deng, J. Alloy. Comp. 554 (2013) 64–71.
[30] V. Kumar, A. Gaur, R.K. Kotnala, J. Alloy. Comp. 551 (2013) 410–414.
[31] A.M. Kadomtseva, Y.F. Popov, A.P. Pytakov, G.P. Vorob'ev, A.K. Zvezdin, D. Viehlands, Phase Transitions 79 (2006) 1019–1042.
[32] C. Ederer, N.A. Spaldin, Phys. Rev. B 71 (2005) 060401.
[33] A.N. Kaveh Ahadi, Seyed-Mohammad Mahdavi, Mater. Lett. 83 (2012) 124–126.
[34] A.H.S.R. Shannigrahi, D. Tripathy, A.O. Adeyeye, J. Magn. Magn. Mater. 320 (2008).